

GAMMA RAYS FROM COMPTON SCATTERING IN THE JETS OF MICROQUASARS:
APPLICATION TO LS 5039CHARLES D. DERMER¹ & MARKUS BÖTTCHER²*Draft version November 10, 2018*

ABSTRACT

Recent High Energy Stereoscopic System (HESS) observations show that microquasars in high-mass systems are sources of very high energy γ -rays. A leptonic jet model for microquasar γ -ray emission is developed. Using the head-on approximation for the Compton cross section and taking into account angular effects from the star's orbital motion, we derive expressions to calculate the spectrum of γ rays when nonthermal jet electrons Compton-scatter photons of the stellar radiation field. The spectrum of Compton-scattered accretion-disk radiation is also derived by approximating the accretion disk as a point source of radiation located behind the jet. Numerical results are compared with simpler expressions obtained using δ -function approximations for the cross sections, from which beaming factors are derived. Calculations are presented for power-law distributions of nonthermal electrons that are assumed to be isotropically distributed in the comoving jet frame, and applied to γ -ray observations of LS 5039. We conclude that (1) the TeV emission measured with HESS cannot result only from Compton-scattered stellar radiation (CSSR), but could be synchrotron self-Compton (SSC) emission or a combination of CSSR and SSC; (2) fitting both the HESS data and the EGRET data claimed to be associated with LS 5039 requires a very improbable leptonic model with a very hard electron energy distribution. Because the γ rays would be variable in a leptonic jet model, the data sets are unlikely to be representative of a simultaneously measured γ -ray spectrum. We therefore attribute EGRET γ rays primarily to CSSR emission, and HESS γ rays to SSC emission. Detection of periodic modulation of the TeV emission from LS 5039 would favor a leptonic SSC or cascade hadron origin of the emission in the inner jet, whereas stochastic variability alone would support a more extended leptonic model. The puzzle of the EGRET γ rays from LS 5039 will be quickly solved with GLAST.

Subject headings: gamma rays: microquasars—radiation processes: nonthermal

1. INTRODUCTION

X-ray binaries with jets, or microquasars, are common in our Galaxy, with ≈ 16 now known (for a recent review see, e.g., Paredes 2005). About one-third are high-mass X-ray binaries (HMXBs), including Cygnus X-1, Cygnus X-3, LS 5039, and LSI+61°303, and the remainder are low-mass X-ray binaries (LMXBs), including GRS 1915+105, GRO J1655-40, Sco X-1, and 1E 1740.7-2942. The compact companions are a mixture of black holes and neutron stars, and the radio activity of the microquasars is about equally divided into persistent and transient behaviors.

Recent observations (Aharonian et al. 2005) made with the High Energy Stereoscopic System (HESS) show that the high-mass microquasar LS 5039 is a source of very high energy (VHE) γ rays in the ≈ 200 GeV – 10 TeV range, confirming its earlier tentative identification with the EGRET source 3EG J1824-1514 (Paredes et al. 2000). A second high-mass microquasar system, LSI+61°303 (V615 Cas), is associated with the COS-B source 2CG 135+01 (Hermesen et al. 1977; Gregory & Taylor 1978) and the EGRET source 3EG J0241+6103 (Kniffen et al. 1997), but is too far north for observations with HESS. The EGRET source 3EG J1824-1514 associated with LS 5039 shows marginal evi-

dence for variability (Torres et al. 2003). In contrast, the EGRET light curve of 3EG J0241+6103, the counterpart to LSI+61°303, is strongly variable (Tavani et al. 1998). Moreover, Massi (2004) performed a timing analysis of the 3EG J0241+6103 data and found a most probable period of 27.4 ± 7.2 days, compared to its 26.5 day orbital period.

Evidence for stochastic and periodic variability of these sources at γ -ray energies would argue in favor of a leptonic microquasar jet model similar to blazar jet models (for recent reviews of microquasar models, see Romero 2005; Fender & Maccarone 2004), especially if the X-ray and γ -ray emissions display correlated variability (Gupta et al. 2005). The importance of Compton scattering of external photons to produce gamma-rays in blazar jets was first considered by Begelman & Sikora (1987) and Melia & Königl (1989) and later, in view of the *Compton Observatory* discoveries, by Dermer et al. (1992) and Sikora et al. (1994). A microquasar jet model differs importantly from a blazar jet model through the addition of the stellar radiation field from the high-mass star and the periodic orbital modulation of the binary stellar system (Georganopoulos et al. 2002; Kaufman Bernadó et al. 2002). Although Casares et al. (2005) claim low significance periodic variability when folding the HESS data for LS 5039 with its orbital period, the EGRET data showed no compelling evidence for either stochastic or periodic variability (Paredes et al. 2000). The X-rays from LS 5039 are, however, moderately variable. *RXTE* observations in the 3 – 30 keV

¹ E. O. Hulburt Center for Space Research, Code 7653, Naval Research Laboratory, Washington, DC 20375-5352

² Astrophysical Institute, Department of Physics and Astronomy, Ohio University, Athens, OH 45701, USA

range may show periodic variability correlated with the periastron passage of LS 5039, so it is uncertain whether the X-rays are associated with accretion disk or the jet (Bosch-Ramon et al. 2005).

In addition to stellar and accretion-disk emissions, microquasar emission from the jet will produce a variable multiwavelength continuum consisting of radio/IR and jet X-ray (Markoff et al. 2001) synchrotron radiation. Nonthermal γ -ray emission is likely to originate from synchrotron self-Compton (SSC) (Atoyan & Aharonian 1999) and external Compton (EC) processes (Levinson & Blandford 1996; Georganopoulos et al. 2002) by these same jet electrons. The bright high-mass star makes an important contribution to the external radiation field in HMXBs, whereas the accretion disk is the dominant external photon source in LMXBs (Grenier et al. 2005a). Compton-scattering leptonic jet models of the γ -ray emission from LS 5039 and LSI+61°303 are presented by Bosch-Ramon & Paredes (2004a,b).

In this paper, we perform a Compton-scattering analysis of the jet γ -ray emission from HMXB microquasars for a leptonic jet model, focusing on Compton-scattering effects from the azimuthal variations of the stellar radiation field using parameters inferred from observations (McSwain et al. 2001; Casares et al. 2005) of LS 5039, which has a period of 3.90603 ± 0.00017 days. We assume that the twin jets of the microquasar are oriented normal to the orbital plane of the compact object and star; geometrical complications of precessing jets are not considered here. The orbital variations of the bright O or B stars introduce interesting kinematic variations that appear in the γ -ray emission spectrum if the γ rays are due to stellar photons that are Compton-scattered by non-thermal jet electrons, including variations of peak νF_ν photon energy and inferences of the locations of the γ -ray emission site. This emission is also subject to the effects of $\gamma\gamma$ absorption (Böttcher & Dermer 2005; Dubus 2005), although this effect is not included in the calculations shown here.

Angle-dependent effects on Compton-scattered jet radiation are treated in Section 2. Approximations made in the derivation are clearly enumerated, so that they can be relaxed in more detailed numerical treatments. In particular, the analysis employs a fixed electron distribution. Spectral calculations are presented in Section 3 using parameters appropriate to LS 5039. Difficulties to fit the combined EGRET and HESS spectra of LS 5039, if assumed to be simultaneously radiated, are discussed in Section 4. Implications for establishing the nature of microquasar γ -ray emission from LS 5039 from further HESS and upcoming GLAST observations are also considered. A summary of the results is given in Section 5.

2. GAMMA RAYS FROM COMPTON-SCATTERED STELLAR RADIATION

The geometry of the microquasar system is shown in Fig. 1. The generic system considered here is a HMXB with parameters taken from observations of LS 5039, but our results are also applicable to LMXBs when the accretion disk is approximated by a hot spot at the base of the twin jets. The star and the compact object, separated by distance d , are assumed to follow circular orbits around

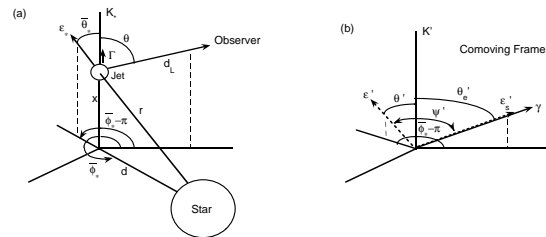


FIG. 1.— Geometry of scattering in the microquasar system. (a) Stationary frame K_* of the microquasar system. The stellar azimuthal angle $\phi_* = 0$ when the high-mass star is closest to the observer. The photon azimuth in the comoving frame is then $\phi_* - \pi$. (b) Comoving frame K' of the jet plasma. In the head-on approximation, the photon is scattered along the direction of the scattering electron. See text for definition of symbols.

their common center of mass. Material from Roche-lobe overflow in low-mass systems, or stellar winds in high-mass systems, forms an accretion disk surrounding the compact object. As the matter accretes onto the neutron star or black hole, plasma is assumed to be ejected transverse to the orbital plane in the form of twin jets.

2.1. Model Assumptions

Given that the dominant radiation mechanism for microquasar γ -ray emission is undecided, for example, whether microquasar emissions have a primary hadronic (e.g., Romero et al. 2003; Aharonian et al. 2005a) or leptonic (e.g., Bosch-Ramon et al. 2005b; Paredes et al. 2005) origin, an overly complicated leptonic jet model for microquasar emission seems unjustified at this time. A number of simplifying assumptions are therefore made that can be relaxed in more detailed treatments. Specifically, we assume that

1. the jets are steady and oriented in the direction normal to the orbital plane of the binary system, with the jet electrons confined to the axis defining the jet direction;
2. the orbit is circular;
3. the star and accretion disk can be treated as point sources of radiation;
4. the nonthermal electrons are isotropically distributed in the comoving frame with a fixed energy distribution, and most of the radiation is emitted at a specified distance above the orbital plane; and
5. cascade processes can be neglected.

Assumption 1 means that we neglect additional periodicities of the jet ejection process possibly associated with periastron passage, or disk precession that could lead to additional modulation of the γ -ray signal. This latter periodicity (e.g., Kaufman Bernadó et al. 2002; Torres et al. 2005) could be different from the orbital periodicity. Moreover, the jets need not be aligned normal to the orbital plane. For example, the jets in V4641 Sgr may lie within $\sim 36^\circ$ of the orbital plane (Butt et al. 2003). These effects can be dealt with in the present

model by treating a more complicated geometry, and X-ray and TeV observations should be cross-correlated to search for periods unrelated to orbital motions. Helical motions of jet trajectories, which may operate in black-hole jet systems (e.g., Rieger 2004), would also require a more detailed treatment than considered here.

Regarding assumption 2, scattering kinematics for highly eccentric orbits can be developed on the basis of the treatment presented here. LS 5039 executes a moderately elliptical orbit in a system with a $22.9 M_\odot$ star of spectral type O6.5, with eccentricity $\cong 0.35$ (Casares et al. 2005). This effect will be displayed in both the scattering kinematics (Paredes et al. 2005) and $\gamma\gamma$ absorption calculations (Dubus 2005), but does not, to first order, change the conclusions we draw by studying anisotropic Compton scattering and $\gamma\gamma$ absorption for circular orbits.

For the purposes of modeling VHE γ -rays, analysis of a microquasar system must take into account the angle-dependence of the stellar and accretion-disk radiation field both in the Thomson and Klein-Nishina (KN) regimes of scattering. Although Georganopoulos et al. (2001) provide a useful method to calculate scattered radiation spectra in the KN regime, it is applicable as presented only to surrounding isotropic radiation fields, and for jets with fixed isotropic electron distributions. Paredes et al. (2005) and Bosch-Ramon et al. (2005b) also treat the anisotropy of the stellar radiation field in a simplified fashion, without fully taking into account the effects of the directional target photon field.

In this work, we treat the angular dependence of Compton-scattered stellar and accretion-disk radiation fields employing an accurate approximation to the Compton cross section in the head-on approximation that is valid throughout the Thomson and KN regimes. To avoid over-complicated expressions, the star and accretion-disk are treated as point sources of photons scattered by nonthermal electrons in a relativistically-moving jet with negligible extent (assumption 3). These assumptions simplify the derivation, but in no way violate the essential geometry of the microquasar system, and are straightforward (if tedious) to relax. Nevertheless, it is important to note that the companion star in a HMXB can subtend as much as $\approx 10\%$ of the full sky as seen from a location close to the compact object.

We also assume a non-evolving electron distribution and calculate emission from a fixed jet location (assumption 4). As the jet plasma moves away from the microquasar system, the electrons are energized, for example, through internal collisions of ejected plasma shells or via shocks formed during interactions of the jetted plasma with the external medium. The nonthermal electrons subsequently lose energy through expansion and radiative losses. In more detailed treatments, electron-energy evolution through synchrotron, Compton, and adiabatic losses are considered (e.g., Atayan & Aharonian 1999; Bosch-Ramon et al. 2005a; Gupta et al. 2005). When stellar radiation fields are important, a consistent treatment of the evolution of the nonthermal electron Lorentz factor distribution with location requires, in addition to the synchrotron, SSC, and adiabatic energy-loss rates, electron energy-loss rates obtained from the Compton-scattered stellar and accretion-disk radiation fields, as derived here. Given that γ -ray telescopes integrate over

a long time to accumulate signal in comparison with Compton and synchrotron cooling time scales for the γ -ray emitting electrons, as is easily demonstrated, the detected emission is well-approximated as the radiation from a time-averaged electron distribution. Yet the power-law form of the electron distribution remains an assumption that may not agree with calculations of electron evolution.

Finally, we do not treat the electromagnetic cascades formed through $\gamma\gamma$ attenuation as γ -rays propagate through the anisotropic radiation field of the jet and star (see, e.g., Protheroe et al. 1992; Bednarek 1997; Aharonian et al. 2005a). Cascading effects could be important when the absorption depth to $\gamma\gamma$ pair production attenuation is large, namely within the inner jet³ (Böttcher & Dermer 2005; Dubus 2005). This effect could, in principle, reduce the level of modulation of the VHE γ -ray signal from $\gamma\gamma$ attenuation and introduce new spectral components. Relaxing assumption (5) introduces, however, new assumptions about the strength and geometry of the magnetic field in the vicinity of the microquasar outside the jet plasma that are difficult to constrain.

2.2. Stellar Radiation Field

We treat a system (Fig. 1a) where the jet outflow has constant bulk Lorentz factor $\Gamma = 1/\sqrt{1-\beta^2}$. In the stationary frame of the microquasar system (where the center-of-mass of the compact object and high-mass star is at rest), the plasma will have traveled a distance $x = \beta ct_*$ from the compact object and reached a distance $r = \sqrt{x^2 + d^2}$ from the companion star after time t_* , measured from the moment of ejection of the jetted plasma at $x = 0$.

Let $\phi_*(t) = \omega_* t_*$ represent the star's orbital phase measured from the angle when the high-mass star is closest to the observer, where $\omega_* = 2\pi/P$ is the star's angular frequency and P is the period (from hours to days for LMXBs, and days to weeks for HMXBs). Photons from the companion star impinge on the outflowing jet plasma at an angle $\bar{\theta}_* = \arccos \bar{\mu}_*$ to the jet axis as measured in the stationary frame of the star, where $\bar{\mu}_* = x/r = 1/\sqrt{1+d^2/x^2}$. The angle $\theta = \arccos \mu$ is the inclination of the observer with respect to the jet axis.

The energy flux at distance r from a uniform brightness sphere (i.e., the star) of radius R_* is

$$\frac{d\mathcal{E}_*}{dAdtd\epsilon_*} = \frac{\pi R_*^2}{r^2} B_{\epsilon_*},$$

where \mathcal{E}_* is the radiated photon energy and $\epsilon_* = h\nu_*/m_e c^2$ is the dimensionless photon energy. The intensity

$$B_{\epsilon_*} = I_{\epsilon_*}^{bb}(\Theta) = \frac{2m_e c^3 \epsilon_*^3}{\lambda_C^3 [\exp(\epsilon_*/\Theta) - 1]}$$

for a blackbody, where $\lambda_C = h/m_e c = 2.42 \times 10^{-10}$ cm is the Compton wavelength of the electron and $\Theta = k_B T_*/m_e c^2$ is the dimensionless temperature of the star.

Consider a star with luminosity L_* and temperature T_* , so that the stellar radius $R_* = \sqrt{L_*/4\pi\sigma_{\text{SB}}T_*^4}$, and

³ Inner jet refers to jet locations $x \lesssim d$.

σ_{SB} is the Stefan-Boltzmann constant. The differential energy density

$$u_{bb}(\epsilon_*, r) = \frac{1}{c} \frac{d\mathcal{E}_*}{dAdtd\epsilon_*}.$$

Hence

$$u_{bb}^*(\epsilon_*, \Omega_*; r) = u_*^0 \frac{\epsilon_*^3 \delta(\mu_* - \bar{\mu}_*) \delta(\phi_* - \bar{\phi}_*)}{\exp(\epsilon_*/\Theta) - 1}, \quad (1)$$

where

$$u_*^0 = \frac{15L_*}{4\pi^5 c \Theta^4 r^2}.$$

The stationary-frame photon density $n_{ph}^*(\epsilon_*, \Omega_*) = u^*(\epsilon_*, \Omega_*)/(m_e c^2 \epsilon_*)$.

The $f_\epsilon^* = \nu F_\nu^*$ spectrum of the star measured by an observer located a (luminosity) distance d_L away from the star is

$$f_\epsilon^* = \frac{15L_*}{4\pi^5 \Theta^4 d_L^2} \frac{\epsilon^4}{\exp(\epsilon/\Theta) - 1}, \quad (2)$$

where $\epsilon = \epsilon_*/(1+z) \cong \epsilon_*$ for the low redshift ($z \ll 1$) sources considered here.

2.3. Stellar Radiation Photons Compton-Scattered by Jet Electrons

The detailed derivation of the Compton-scattered stellar radiation (CSSR) spectrum is given in Appendix A. The νF_ν spectrum resulting from Compton-scattered stellar radiation (CSSR) for a uniform emitting region filled with an isotropic comoving distribution of electrons is

$$f_\epsilon^{C*} = \frac{3c\sigma_T u_*^0 \delta_D^2 \epsilon^2}{32\pi d_L^2} \int_{\epsilon/\delta_D}^{\infty} d\gamma \frac{N'_e(\gamma)}{\gamma^2} \times \\ a^2 \left[g^{-2} (y + \frac{1}{y}) I_1 - \frac{2\epsilon}{\delta_D \gamma y b g} I_2 + \left(\frac{\epsilon}{\delta_D \gamma y b} \right)^2 I_3 \right] \quad (3)$$

where $y = 1 - (\epsilon/\delta_D \gamma)$,

$$\delta_D = [\Gamma(1 - \beta\mu)]^{-1}, \quad (4)$$

is the Doppler factor, $\epsilon = h\nu/m_e c^2$ is the dimensionless observed photon energy, $N'_e(\gamma)$ is differential distribution of electrons with comoving Lorentz factors γ , and d_L is the luminosity distance to the source. The functions a , b , I_1 , I_2 and I_3 are defined in Appendix A.

2.4. Compton Spectrum from Point Source of Radiation Field Behind Jet

The accretion disk provides a source of external radiation that enters the jet from behind. For a Shakura-Sunyaev accretion disk, the distance where the transverse extent of the accretion disk can be neglected and the accretion disk can be approximated by a point source is given by

$$x \gg \Gamma^4 r_g \quad (5)$$

(Dermer & Schlickeiser 1993, 2002), where $r_g = GM/c^2$ is the gravitational radius of the black hole with mass M . For the mildly relativistic speeds ($\Gamma \approx 1 - 2$) considered here, and jet distances of order of the orbital radius, the accretion disk can be well approximated as a point source of radiation. The accretion-disk radiation spectrum may not be well represented by a blackbody or a

Shakura-Sunyaev spectrum, as accretion disks display a wide range of spectra. This does not affect eq. (5), as this estimate is based on energy dissipation at various radii, which is largely unaffected by disk type.

Following the procedure in Appendix A, again using the head-on approximation, eq. (A4), for the Compton cross section, but now for a point source at the origin, we derive the νF_ν spectrum of Compton-scattered accretion disk (CSAD) radiation given by

$$f_\epsilon^{pt} = \frac{3\epsilon^2 \delta_D^2 \sigma_T}{128\pi^2 x^2 d_L^2} \int_0^\infty d\epsilon_0 \frac{L_0(\epsilon_0)}{\epsilon_0^2} \int_{\gamma_{min}}^\infty d\gamma \frac{N'_e(\gamma)}{\gamma^2} \times \\ \left[y + y^{-1} - \frac{2\epsilon}{\delta_D \gamma \hat{\epsilon}_i y} + \left(\frac{\epsilon}{\delta_D \gamma \hat{\epsilon}_i y} \right)^2 \right], \quad (6)$$

where $\hat{\epsilon}_i = \gamma \epsilon_0 \delta_D (1 - \mu)$ and

$$\gamma_{min} = \frac{\epsilon}{2\delta_D} \left[1 + \sqrt{1 + \frac{2}{\epsilon_0(1 - \mu)}} \right].$$

Appendix B gives approximate expressions for the CSSR and CSAD spectra in the Thomson and KN regimes that reduce the number of numerical integrations, though at the expense of accuracy. These simpler expressions have, however, the virtue of allowing the beaming factors of the various processes to be simply derived.

3. RESULTS

We calculate the CSSR spectrum using the standard parameters listed in Table 1. The standard jet height x is taken to be equal to the mean orbital separation $d = 2.5 \times 10^{12}$ cm of LS 5039. We also employ a broken power-law distribution for the nonthermal electrons, given by

$$N'_e(\gamma) = K [\gamma_1^{q-p} \gamma^{-q} H(\gamma; \gamma_0, \gamma_1) + \gamma^{-p} H(\gamma; \gamma_1, \gamma_2)]. \quad (7)$$

Normalizing to the total comoving nonthermal electron energy

$$W'_e \cong m_e c^2 \int_1^\infty d\gamma \gamma N'_e(\gamma)$$

gives

$$K = \frac{W'_e}{m_e c^2} \left[\frac{\gamma_1^{q-p} (\gamma_1^{2-q} - \gamma_0^{2-q})}{2-q} + \frac{\gamma_1^{2-p} - \gamma_2^{2-p}}{p-2} \right]^{-1}. \quad (8)$$

The maximum electron Lorentz factor is calculated from the well-known (Guilbert et al. 1983) radiation-reaction limit obtained by equating the electron energy-loss timescale with the gyration timescale $t_g = m_e c \gamma / eB$, which holds provided that synchrotron losses dominate Compton-energy losses. The situation is more complicated here, where Compton-losses from the stellar radiation field are large and KN effects are important (Aharonian et al. 2005a). In Appendix C, an improved treatment of this limit for relativistic jets is performed, and we quantify the regime where the synchrotron radiation-reaction limit holds. We take $\gamma_2 = \gamma_{max}$ here, with γ_{max} given by eq. (C1) and $\eta = 1$, giving the most optimistic maximum synchrotron frequency.

Fig. 2 show calculations of the νF_ν SED of the CSSR process. The dependence of the SED on phase of the binary orbit is shown in Fig. 2a, and the dependence of the SED on various parameters of the binary system at $\phi = \pi/2$ is shown in Fig. 2b (we now simplify the notation

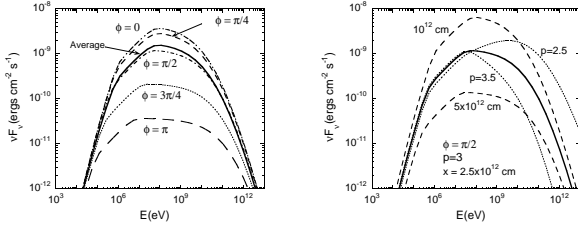


FIG. 2.— The νF_ν Compton-scattered stellar radiation (CSSR) spectral energy distribution (SED) from a microquasar jet when nonthermal jet electrons Compton-scatter photons of the high-mass companion star. Standard parameters of the system, appropriate to LS 5039, are given in Table 1. In particular, the jet height above the orbital plane of the system is assigned a standard value of $x = 2.5 \times 10^{12}$ cm, the jet plasma outflow Lorentz factor $\Gamma = 2$, and the number index of the electron energy distribution is $p = 3$. (a) Dependence of the SED on phase ϕ , with $\phi = 0$ when the companion star is nearest the observer (Fig. 1a). The average SED integrated over all phases is shown by the solid curve. (b) Dependence of the CSSR SED on x and p with $\phi = \pi/2$. The solid curve shows the SED for the standard parameters, and the other curves are labeled with the parameter that has changed from the standard parameter values. Effects of $\gamma\gamma$ attenuation on the SEDs are not included here.

by letting the stellar azimuth angle $\bar{\phi}_* \rightarrow \phi$). In both figures, the steep lower energy behavior is a consequence of the low-energy cutoff Lorentz factor $\gamma_0 = 100$ assumed in the electron distribution. The energy of this low-energy cutoff, and the cutoff associated with the change in slope at $\gamma_1 = 10^3$, occurs for the blackbody stellar spectrum around photon energy

$$E_T \cong 2.7 k_B T_* \gamma_i^2 \delta_D \Gamma (1 - \beta \bar{\mu}_*) (1 - \cos \bar{\psi}'), \quad i = 0, 1, \quad (9)$$

provided that the scattering takes place in the Thomson regime. (This result is found from the δ -function approximations for Thomson scattering given in Appendix B.) Except for the phase-dependent factor $(1 - \cos \bar{\psi}')$, all the terms in eq. (9) are uniquely determined. For the standard parameters of Table 1, $\beta = 0.866$, $\delta_D = 2.32$ and $\bar{\mu}_* = 0.707$, so that the breaks due to Thomson scattering occur at $E_\gamma \cong 16 \gamma_i^2 (1 - \cos \bar{\psi}') \text{ eV}$, in accord with the results shown. The breaks in the photon spectrum in Fig. 2a occur at lower energies when $\phi = \pi$ than when $\phi = 0$ because the $\phi = \pi$ case involves more nearly tail-on scattering events that scatter the target photons to lower energies than for the more nearly head-on scattering events with $\phi \approx 0$ (see Fig. 1a).

The spectral index of the Compton-scattered stellar radiation follows the well-known behavior

$$\alpha_\nu = \frac{3 - p}{2}$$

in the Thomson regime, as shown in Appendix B, where α_ν is the νF_ν spectral index⁴. For electron index $p = 2$ assumed in the lower branch of the electron spectrum in Fig. 2a, the spectrum rises with slope 1/2 in a νF_ν plot. For the upper branch of the electron spectrum with $p = 3$, the spectrum is flat, as seen for the $\phi = \pi$ curve in Fig. 2a. For the more nearly head-on scattering events

⁴ At lower energies, $\alpha_\nu \cong 2$, corresponding to the low-energy emissivity spectrum $j' \propto \epsilon'$ of a mono-energetic electron distribution (Blumenthal & Gould 1970).

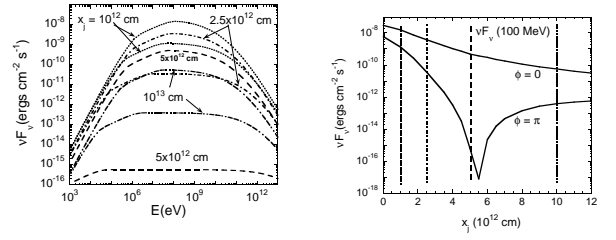


FIG. 3.— The νF_ν CSSR SED as a function of jet height x at phases $\phi = 0$ and π , for standard parameters given in Table 1. (a) Dependence of the SED on x at phases $\phi = 0$ and $\phi = \pi$ shown in the upper and lower curves, respectively, of each pair. (b) The value of νF_ν at 100 MeV at $\phi = 0$ and $\phi = \pi$. Effects of $\gamma\gamma$ attenuation on the SEDs are not included here, but is unimportant below $\approx 50 \text{ GeV}$.

with $\phi \approx 0$, the transition to the KN regime occurs at lower photon energies, so that scattering in the Thomson regime is never fully achieved. Indeed, the CSSR spectral index at high-energies asymptotically approaches the steep KN index $\alpha_\nu \approx 1 - p$ (eq. [B9]).

Transition to the KN regime of scattering, as derived in Appendix B, takes place over a broad range of photon energies centered around⁵

$$E_{\text{KN}} \cong \left(\frac{m_e c^2}{4 \times 2.7 \Theta} \right) \times \frac{\delta_D}{\Gamma (1 - \beta \bar{\mu}_*)} \times \frac{1}{(1 - \cos \bar{\psi}')} \cong \frac{20 \text{ GeV}}{(1 - \cos \bar{\psi}')} \quad (10)$$

The three terms making up the middle expression represent, from left to right, the transition energy for a monochromatic radiation field with mean photon energy $\approx 2.70 \Theta m_e c^2$, a factor for the dependence on jet speed, stellar location and observer direction, and an angular factor accounting for the stellar azimuth. The $\phi = 0$ and $\phi = \pi$ cases in Fig. 2a have, roughly, $\cos \bar{\psi}' \sim -0.9$ and $\cos \bar{\psi}' \sim +0.8$, which accounts for the large ranges in photon energies corresponding to the transition to the KN behavior. KN effects are quite substantial, however, even at lower energies than given by eq. (10), because of the gradual change in the Compton cross section over the range where recoil effects start to become important.

Because the transition to the KN regime occurs at lower values of scattered photon energy at $\phi = 0$ where the flux is higher than for the $\phi = \pi$ case where the flux is lower, the CSSR process will produce a softer spectra with increasing flux at multi-GeV – TeV energies. This is the same behavior as inferred from the effects of $\gamma\gamma$ absorption on the emitted radiation spectrum (Böttcher & Dermer 2005), and so would enhance this behavior.

Besides the rapid transition to the steep KN behavior at energies $\lesssim 100 \text{ GeV}$, Fig. 2a shows that the CSSR spectra are strongly modulated in flux as a function of phase of the binary system. Also shown in Fig. 2a by the solid curve is the phase-averaged CSSR SED, which is approximately equal to the $\phi = \pi/2$ curve (actually closer to $\phi \cong 7/16$). Fig. 2b shows calculations of CSSR at $\phi = \pi/2$ for different values of p and x . Due to

⁵ The factor 1/4 is introduced because the domain of Compton scattering is defined by the value of the quantity $4\gamma\epsilon'$ rather than $\gamma\epsilon'$; see Blumenthal & Gould (1970).

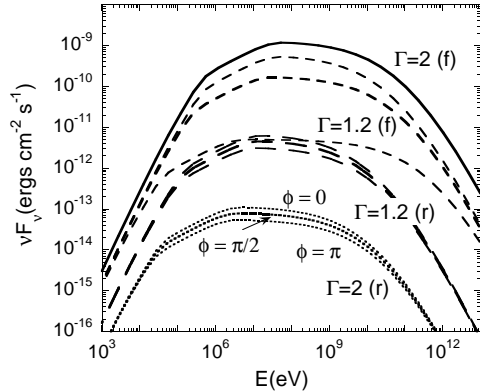


FIG. 4.— Dependence of the CSSR SED of a two-sided jet on the bulk Lorentz factor Γ of the plasma. The SEDs for the forward (f) and reverse (r) jets are shown for $\Gamma = 1.2$ and $\Gamma = 2$ at phases $\phi = 0, \pi/2$, and π (see Table 1 for parameters). Only the $\phi = \pi/2$ curve is shown for the $\Gamma = 2$ forward jet; the other phase-dependent spectra for this case are shown in Fig. 2a.

the diminution of the target photon density, the absolute value of the flux decreases rapidly with jet height x , as expected. The harder electron spectrum causes the peak of the CSSR SED to shift to higher energies, but the spectrum still falls rapidly when KN effects become important.

Fig. 3 shows in more detail how the CSSR SED depends on jet height x at phases $\phi = 0$ and π . For these parameters, the νF_ν spectrum peaks between 100 MeV and 1 GeV, as shown in Fig. 3a. If γ -ray emission from microquasars is due to this process, then strong phase-dependent modulation is expected if the jet electrons radiate on a distance scale comparable to the orbital radius. As seen in Fig. 3b, the CSSR flux nulls at $\phi = \pi$ when the inclination angle $\theta \cong \arctan(d/x)$, which takes place at $x \cong 5.4 \times 10^{12}$ cm for our parameters. This happens because the target photons are directed almost exactly “tail-on” past those electrons which would scatter photons into our observing direction. This effect will be somewhat ameliorated in calculations where the star has a finite extent.

Unlike the $\gamma\gamma$ attenuation process, which ceases to be effective at producing even 10% orbital modulation of the VHE emission when $x \approx 10^{13}$ cm (Böttcher & Dermer 2005), the CSSR process will produce significant phase-dependent modulation of the ~ 100 MeV – GeV emission to much larger distances. The 100 MeV fluxes at $\phi = 0$ and $\phi = \pi$ differ by a factor of 2 at $x \approx 5 \times 10^{13}$ cm, and by a factor of 10% at $x \approx 5 \times 10^{14}$ cm. Therefore even if the γ -ray emission is not produced in the inner jet, GLAST could still detect significant orbital modulation of the γ rays. The large range of distances that produce significant orbital modulation also makes the claim (Massi 2004) of periodic variability of the EGRET emission from 3EG J0241+6103 associated with LSI+61°303 more believable, and suggests that the EGRET data for 3EG J1824-1514 should be reanalyzed to establish strong limits to modulation at the orbital period of LS 5039.

Fig. 4 illustrates the dependence of the fluxes of a two-sided jet for model jets with $\Gamma = 1.2$ and 2. The forward (f) jets are inclined at $\theta = 25^\circ$ to the observer, and

the reverse (r) jets have $\theta = 155^\circ$. Even at mildly relativistic Lorentz factors, the Doppler boosting can lead to differences of several orders of magnitude between the fluxes from the forward and reverse jets. As shown in Appendix B, the beaming factors for Thomson-scattered radiation for external photons that enter the jet from behind and in front of the jet are $\propto \delta_D^{3+p}(1-\mu)^{(p+1)/2}$ and $\propto \delta_D^{3+p}(1+\mu)^{(p+1)/2}$, respectively. For the standard parameters, $\mu = 0.9063$, $p = 3$, and $\beta = 0.866$ for $\Gamma = 2$. Thus the ratio of scattered fluxes of the forward and reverse jets range from ≈ 800 for target photons entering from behind, to $\approx 10^8$ for target photons entering from in front of the jet. Intermediate values are found for stellar photons that enter at shallow angles, as calculated in Fig. 4. This shows that CSSR from the reverse jet can generally be neglected for even mildly relativistic jets.

4. COMPTON-SCATTERING LEPTONIC JET MODEL FOR LS 5039

In this section, we apply the preceeding results to LS 5039 data, showing that

- It is very difficult to fit the HESS with a CSSR model because of the strong curvature produced by KN effects;
- An improbable leptonic model with electrons accelerated with maximum efficiency with a distribution displaying no spectral breaks is required to fit both EGRET and HESS data, assuming that these data are representative of the simultaneously measured spectrum of LS 5039;
- The EGRET and HESS data can be separately fit with emission that is primarily from the CSSR and SSC processes, respectively, which implies significant aperiodic variability of the γ rays.

We furthermore consider other possible origins for the broadband emission from LS 5039, including hadronic and combined hadronic and leptonic models, and the possibility that the EGRET emission associated with LS 5039 originates from another source in the LS 5039 field, or is contaminated by, e.g., diffuse radiation.

Fig. 5 shows non-simultaneous data (Aharonian et al. 2005) taken at radio, optical, X-ray, and γ -ray wavelengths, with EGRET data points taken from Bosch-Ramon & Paredes (2004a). The HESS data are described by a power-law spectrum between 250 GeV and 4 TeV with photon index $= 2.1 \pm 0.15$ (Aharonian et al. 2005). We find that fitting the HESS spectrum with a pure CSSR model faces severe difficulties. This is due to the strong KN decline and marked convexity of the CSSR radiation spectrum at TeV energies. Extremely hard ($p \approx 2$) electron spectra extending to very high energies are required for such a model to work, but in all cases the CSSR SEDs display strong curvature that should be measurable with more sensitive HESS data.

Assume now that the EGRET and HESS data represent the γ -ray spectrum of LS 5039 that would be measured at a single epoch. In order to fit both the EGRET and HESS data simultaneously, we find that a CSSR fit to the EGRET data will produce too soft of a spectrum in the HESS range. This is likewise the case for an SSC model fit to the EGRET data. A leptonic SSC model

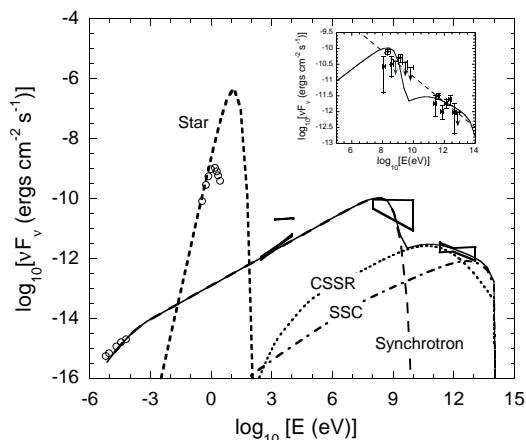


FIG. 5.— Leptonic jet model fit for the LS 5039 data, using Model A parameters given in Table 1. The low and high X-ray spectra are from XMM and RXTE observations, respectively. The optical data have not been dereddened. This figure illustrates the difficulty that leptonic jet models have to fit the joint nonsimultaneous EGRET and HESS data if these data are assumed to represent the broadband LS 5039 γ -ray spectrum measured at a single epoch. Inset shows the fit to the EGRET and HESS data in more detail, with the dashed line indicating the small range of power-law spectra that connect the EGRET and HESS data. Total spectrum is shown by the solid curve, with components as labeled.

can fit the HESS data alone, as we show below. But an SSC model fit to the HESS data means that the EGRET data require a separate explanation. One possibility considered in Fig. 5 is that the high-energy extension of the synchrotron spectrum could produce emission in the EGRET band. For the hard synchrotron spectrum required in this case, it is then necessary to fine-tune the joint CSSR and SSC spectra to obtain an acceptable fit to the joint EGRET and HESS data (see inset of Fig. 5). Model A parameters given in Table 1 are used in this fit, noting that the mean magnetic field $B \lesssim 10$ G in order to have sufficiently energetic electrons to scatter target photons to multi-TeV energies (eq. [C1]).

It is interesting to note that the radio and low-state X-ray emission from LS 5039 can be connected by a single power-law. This suggests that the radio through X/ γ -ray emission could originate from the same (non-thermal jet synchrotron) process, as has been argued to be the case for models of the LMXBs XTE J1118+480 (Markoff et al. 2001) and GX 339-4 (Markoff et al. 2003) on the basis of radio, IR, and X-ray spectral correlations. In those models, a broken power-law jet synchrotron radiation spectrum resulting from adiabatic and radiative cooling is used to fit the data. A similar type of model, as shown in Fig. 5, could in principle fit the radio/low-state X-ray data from LS 5039 if the synchrotron cooling frequency lies either below radio frequencies or above ~ 100 MeV γ -ray energies.

Nevertheless, we do not consider this a viable explanation, as it requires acceleration of electrons with maximal efficiency (eq. [C1]) with no strong evidence for a synchrotron cooling break from the radio through ~ 100 MeV γ -ray regime. It also requires fine-tuning of the CSSR and SSC spectra to fit the HESS data. Moreover,

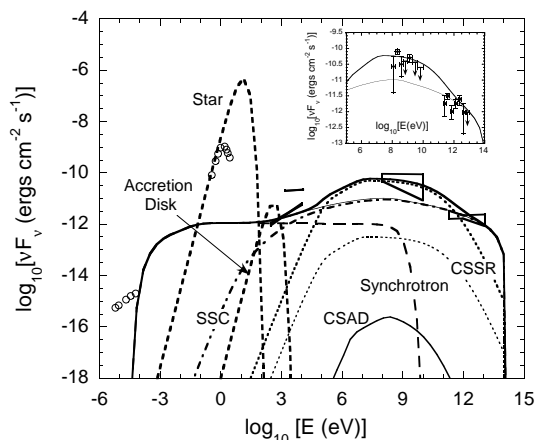


FIG. 6.— Leptonic jet model fit for the LS 5039 data, using Model B parameters given in Table 1. The heavy and light solid curves in the main panel and inset gives the total spectra for Model B parameters with $x = 10^{13}$ cm and $x = 10^{14}$ cm, respectively.

in this jet model, as well as in the models by Markoff et al., the radio emission begins to be self-absorbed below ~ 10 GHz (see Fig. 5) for a comoving jet radius $r_b = 2 \times 10^{11}$ cm (Table 1) needed to give the requisite SSC flux. The radio data of LS 5039, by contrast, shows no evidence for self-absorption.

Thus if the EGRET and HESS data are to be jointly fit, it seems that a leptonic jet model does not work. Yet a simple hadronic model, where the emission is due to a power-law spectrum of cosmic rays accelerated by the outer parts of the jet, which then interact with the ambient medium or the dense matter field of the stellar wind (Romero et al. 2003) to produce secondary nuclear pion-decay γ rays, seems no more likely. The dot-dashed line connecting the EGRET and HESS data in the inset to Fig. 5 suggests that a single power law with number index $\simeq 2.4$ nearly connects the two data sets. But a power-law cosmic-ray spectrum produces a convex γ -ray spectrum at a few hundred MeV due to the pion production and decay processes (Romero et al. 2005) that would miss the EGRET data points which are most significant.

Any leptonic jet model would predict stochastic variability, so clearly the assumption that needs to be relaxed is that the EGRET and HESS data, taken years apart, are typical of a contemporaneously measured data set. Leptonic jet models must be highly variable in view of the short radiative cooling times of nonthermal jet electrons, which require active mechanisms for accelerating the electrons, such as internal shocks from variable relativistic plasma outflows that form the microquasar jets.

Fig. 6 shows an example of a fit where the EGRET data are due primarily to the CSSR process, and the HESS data are due primarily to the SSC process. Here we take $r_b = 10^{11}$ cm. The spectral components, and the heavy solid and dotted curves for the CSSR process and the total spectrum, respectively, refer to the case when $x = 10^{13}$ cm. The light solid curve for the total spectrum and the light dotted curve for the CSSR process refers to the case when $x = 10^{14}$ cm. All other parameters remain

the same (we let $\phi = \pi/2$ in our fits). The difference between the two spectral fits are then due to the effects on the CSSR component arising from the different distances of the jet from the star. We do not fit the radio emission, which is produced at scales as large as ~ 1000 AU (Paredes et al. 2000, 2002).

Also shown for completeness is a model accretion-disk spectrum with emission that is comparable to the low-state X-ray flux, along with the associated CSAD radiation. When $x \gg 10^{12}$ cm, the CSAD process makes no significant contribution to the γ -ray emission. It is surprising, however, how weak and soft (here we use an effective temperature of 0.3 keV) the accretion-disk radiation field has to be in comparison with the flux level of the jet radiation, and even here the model overproduces the low-state X-ray observations. The use of more realistic disk models with hard X-ray emissions could better fit the low-state X-ray data, as observed with XMM-Newton, as well as X-ray states measured with RXTE (Bosch-Ramon et al. 2005), though these authors favor a jet origin for the X-rays in view of the spectral index/flux correlation and the smooth transition that is indicated between the X-ray and γ -ray components (the X-ray high state shown in Figs. 5 and 6 represent the historical 1998 high fluxes measured with RXTE, but may be contaminated by diffuse emission; see Ribó et al. 1999; Bosch-Ramon et al. 2005).

Fig. 6 shows that if the CSSR process accounts for the origin of the γ rays measured with EGRET, then it would exceed the flux measured by HESS at photon energies of several hundred GeV. This can be reversed to make a prediction that when the emission from LS 5039 is luminous in the ~ 100 MeV – GeV band, then the HESS spectrum will be brighter and softer than reported by Aharonian et al. (2005). Besides predicting stochastic variability, our model would also predict weak or absent periodic variability of the HESS emission on the orbital timescale associated with the SSC emission process. This is because SSC emission does not exhibit (for fully isotropized electron distributions) the periodic emission signatures of the CSSR process. There could, however, be variability of the HESS emission on the orbital timescale due to $\gamma\gamma$ effects if the SSC emission originated from the inner jet, which would display the distinctive features that we recently calculated (Böttcher & Dermer 2005). Aperiodic variability of the γ ray emission could arise from a region as large as ~ 10 AU, corresponding to the size scale of resolved, radio emission from LS 5039. The size scale of the γ -ray emission would be difficult to constrain unless sub-hour variability were measured with HESS or GLAST. Note that the $\lesssim 1'$ resolution of HESS corresponds, at 2.5 kpc, to $\lesssim 100$ AU. EGRET localized sources in the Milky Way's disk to $\approx 1^\circ$ at best, whereas GLAST will achieve a localization by a factor ≈ 10 better than EGRET.

The situation is, of course, more complicated, and we can consider a number of other possibilities to explain the broadband spectrum of LS 5039. For example,

1. A model involving hadronic cascades from an inner jet source might fit the data. The model of Aharonian et al. (2005a) would predict strong phase-dependent modulation of the γ -rays; if this is not detected with HESS, this model will probably

be ruled out. A more probable hadronic model, in accord with indications of variability, involves the interaction of cosmic-ray accelerated particles with the stellar wind (Romero et al. 2003), though the energetics could be demanding if the cosmic rays diffuse rapidly away from the source.

2. A combined leptonic and hadronic model could explain the observations. In such a model, the ~ 100 MeV – GeV γ rays are due to CSSR with a soft (cooling) electron spectrum with $p \gtrsim 3$, and the VHE γ rays would be formed by a hadronic emission component due to secondary nuclear production with particles from the surrounding medium or stellar wind, as in the model of Romero et al. (2005). In this case, we would expect variable modulated emission at GLAST energies, and non-varying or slowly varying radiation at TeV energies with no periodic modulation. One would also expect extended VHE emission around LS 5039 as the accelerated cosmic rays diffuse away from the source. In contrast, LS 5039 emission is reported to be consistent with a point source (Aharonian et al. 2005); even if the extended VHE emission were too weak to detect with HESS, an associated radio halo from pion-decay secondaries would be expected if a dense target, such as a molecular cloud, was nearby (Bosch-Ramon et al. 2005c).
3. The EGRET emission could originate from another source in the field of LS 5039. Both PSR B1822-14 and SNR G16.8-1.1, the association proposed by Torres et al. (2003), are within the EGRET error box (Aharonian et al. 2005). It is doubtful that a hadronic SNR component could produce the EGRET emission without also being a significant HESS source, so that emission from a pulsar seems more likely. Cosmic ray irradiation of clumped cold dust not recognized in CO surveys (Grenier et al. 2005b) could also masquerade as a γ -ray source in the LS 5039 error box. Because EGRET source detection depends sensitively on the cosmic-ray induced diffuse background, incorrect background subtraction for EGRET, which has a much larger spatial resolution than HESS, could give an incorrect flux for the LS 5039 source. Insofar as LS 5039 is a VHE source, we would still expect it to radiate in the ~ 100 MeV – GeV band, though possibly at a flux level lower than reported by EGRET.

In spite of these possibilities, we think that emission from a leptonic jet is the most likely explanation for the origin of the γ -ray emission from LS 5039 and other galactic microquasars. We agree with Bosch-Ramon & Paredes (2004a) that the EGRET γ rays are likely dominated by CSSR; indeed, a model where the EGRET emission is primarily fit with an SSC component gives a poor fit to the HESS data (Paredes et al. 2005). More likely, the VHE emission observed with HESS is mainly SSC radiation.

5. SUMMARY AND CONCLUSIONS

In this work, we developed a leptonic model for the VHE emission observed from LS 5039 with HESS, where

the Compton-scattered flux depends on observer angle θ , bulk Lorentz factor Γ , and the parameters of the binary microquasar system. If the γ -ray flux of a galactic microquasar is due to stellar photons that are Compton-scattered by jet electrons, then the γ -ray spectrum will exhibit variability correlated with orbital phase of the companion star. The fractional modulation depends strongly on the location of the jet. Phase-dependent modulation of the γ rays can result both from the CSSR process and $\gamma\gamma$ pair-production absorption (Böttcher & Dermer 2005; Dubus 2005) of jet γ rays that interact with photons of the high-mass star. Periodic modulation of the VHE emission with signatures characteristic of the $\gamma\gamma$ attenuation would provide strong evidence in favor of an inner jet model for the origin of VHE γ radiation from LS 5039, whereas variability of the ~ 100 MeV – GeV emission on the orbital timescale allows the γ rays to originate from either the inner or extended ($d \lesssim x \lesssim 100d$) jet.

Our study of the CSSR process for high-mass microquasars yielded a number of results:

1. The high flux states associated with the orbital modulation of the binary microquasar system exhibit stronger spectral softening than the low flux states as a result stronger KN effects near orbital phase $\phi = 0$ than at phase $\phi = \pi$;
2. An expression was derived, eq. (9), relating breaks in the CSSR spectra for scattering in the Thomson regime to breaks in the electron distribution. These breaks can potentially be inferred from the synchrotron radiation spectrum, and used to test a CSSR model.
3. Another expression, eq. (10), was derived that gives the photon energy for the onset of KN effects in CSSR spectra. The KN softening can appear at energies less than $\sim m_e c^2 / (4 \times 2.7\Theta) \sim 25 \text{ GeV} / T_*(\text{eV})$, even for mildly relativistic outflows, due to the gradual onset of the decline in the Compton cross section.
4. Beaming factors for the CSSR process were derived in Appendix B, and it was shown that the principal dependence of the CSSR νF_ν flux $f_\epsilon \propto \delta_D^{3+p}$ (eqs. [B6] and [B9]) for an electron spectrum with index p .
5. Ratios of CSSR fluxes from forward and reverse jets for a microquasar system were obtained. Even for mildly relativistic outflows ($\Gamma \sim 1.5$) of microquasar jets, the ratios of the CSSR fluxes from the forward and reverse jets can be many orders of magnitude.
6. Allowed ranges of parameters related to maximum electron energies permitted by competing Compton losses and measured ratios of Compton-to-synchrotron fluxes were derived in Appendices C and D, respectively, showing that a leptonic inner jet must be, at least, mildly relativistic.
7. Significant modulation of the CSSR γ rays with the orbital period of the star can take place for emission produced in the extended jet, unlike the

modulation produced by $\gamma\gamma$ attenuation, which is only important for emission produced in the inner jet.

From these results, we tried to construct a purely leptonic model for the multiwavelength SED of LS 5039. The HESS data cannot be fit with the CSSR process alone due to the strong curvature of the scattered spectra. If the CSSR process is used to fit the EGRET data, then it overproduces the emission in the HESS band. Thus, it is difficult for the CSSR and SSC processes to fit both the HESS and EGRET data simultaneously. To circumvent this difficulty, we considered a model, Fig. 5, where the EGRET emission is due to nonthermal synchrotron radiation emitted by an electron distribution with a very hard spectrum ($p \lesssim 2.5$) that extends to the radiation-reaction limited maximum electron energy. Not only is this electron distribution unrealistic by displaying no cooling break, but the model requires fine-tuning of the CSSR and SSC processes to fit the HESS data.

Because leptonic jet models should exhibit marked aperiodic variability, it is doubtful that the HESS and EGRET data are representative of the γ -ray spectrum at a fixed epoch. Abandoning this assumption makes it feasible to fit the EGRET data with CSSR emission (Fig. 6) and the HESS data with SSC emission (as in the model of Atoyan & Aharonian 1999). This leptonic model predicts stochastic variability of the HESS data, and enhanced emission at several hundred GeV energies when the ~ 100 MeV – GeV emission is in a high-flux state. The level of modulation of the AGILE/GLAST and HESS γ -ray flux on the stellar orbital period will directly imply the location of the γ -ray emission site; in the former case from the inner or extended jet, and for the latter case, from within the inner jet. Absence of periodicity of the γ -ray emission measured with both GLAST and HESS means that the γ rays originate from the outer ($x \gtrsim 100d$) jet. Confirmation of a leptonic jet model can be made by comparing contemporaneous X-ray and γ -ray observations with predictions of correlated variability (Gupta et al. 2005).

If the jet flow is nonrelativistic, then the jet emission must be produced in the extended or outer jet in order that electrons can be accelerated to sufficiently high energies to emit multi-TeV γ rays (see Appendices B and C). Thus, if the outflows forming galactic microquasar jets are nonrelativistic throughout the full extent of the jet, only weak periodic modulation from Compton scattering, and essentially no periodic modulation from $\gamma\gamma$ absorption effects, is possible. A mildly relativistic ($\Gamma \gtrsim 2$) leptonic jet model in the inner regions of the jet is compatible with the acceleration of sufficiently energetic electrons to make VHE γ rays throughout the HESS band. If HESS data show variability on the orbital timescale, it means that microquasars eject relativistic flows, which must then be decelerated to nonrelativistic speeds by the time the jets are detected with radio telescopes. Jet deceleration can be accomplished through radiative drag on the stellar radiation field—which makes the γ rays—as well as via interactions with the surrounding medium to form shocks that could accelerate cosmic rays. In this case, the radiative opacity should be large and a light pair jet might be required.

The most serious limitation of our study is the use of fixed electron energy distributions. In more realistic models, power-law distributions of nonthermal electrons are accelerated through shock processes and are injected and evolve through radiative, adiabatic, and cascade processes (Atoyan & Aharonian 1999; Bosch-Ramon et al. 2005b) while the jet plasma flows away from the central star. To treat such a system, electron energy-loss rates associated with Compton interactions in both the Thomson and KN regimes need to be derived for use in an equation for electron energy evolution (see Gupta et al. 2005, for an analytic treatment in the Thomson regime). Systems where Compton losses dominate synchrotron losses can introduce unusual hardenings in the steady-state electron distribution and synchrotron spectrum (Dermer & Atoyan 2002), so that it is not clear under what conditions the assumption of a power-law electron distribution is valid. Future work will address this question.

In summary, we have developed a leptonic jet model for galactic microquasars to fit the EGRET and HESS γ -ray data for LS 5039, complementary to the leptonic jet

models developed by Bosch-Ramon et al. (2005a). This model predicts aperiodic variability, and periodic variability correlated with the orbital motion of the star that depends on the location of the γ -ray emission site and the speed of the jet outflow. Joint observations with AGILE, GLAST and air Cherenkov telescopes will quickly reveal the actual contemporaneous γ -ray spectra of high-mass microquasars, their variability properties, and whether a joint CSSR/SSC model, as proposed here, is correct.

We thank V. Bosch-Ramon for a thorough reading of the paper and many useful suggestions. We also thank K. E. Mitman for assistance during the start of this project, G. Romero for comments and S. Gupta for corrections, and G. Dubus and M. de Naurois for helpful correspondence concerning the HESS data. The work of C. D. D. is supported by the Office of Naval Research and the NASA GLAST Science Investigation DPR-S-1563-Y. The work of M. B. is supported by NASA through XMM-Newton GO grant no. NNG04GI50G and INTEGRAL theory grant NNG05GK59G.

APPENDIX

DERIVATION OF CSSR SPECTRUM

Quantities in the comoving jet frame are denoted by primes⁶. The invariance of $u^*(\epsilon_*, \Omega_*)/\epsilon_*^3$ implies that the spectral energy density of the stellar radiation field in the comoving fluid frame is $u'(\epsilon', \Omega') = (\epsilon'/\epsilon_*)^3 u_{bb}^*(\epsilon_*, \Omega_*)$, where $\Omega_* = (\arccos \mu_*, \phi_*)$,

$$\epsilon_* = \Gamma \epsilon' (1 + \beta \mu') , \quad \mu_* = (\mu' + \beta)/(1 + \beta \mu') , \quad \text{and } \phi' = \phi_* - \pi .$$

The reverse transformations are

$$\epsilon' = \Gamma \epsilon_* (1 - \beta \mu_*) , \quad \mu' = (\mu_* - \beta)/(1 - \beta \mu_*) , \quad \text{and } \phi_* = \phi' + \pi .$$

Eq. (1) becomes

$$u'_{bb}(\epsilon', \Omega') = u_*^0 \frac{\epsilon_*^3 \delta(\mu' - \mu'_*) \delta(\phi' - \bar{\phi}_*)}{\Gamma(1 + \beta \mu') [\exp(\epsilon_*/\Theta) - 1]} , \quad (\text{A1})$$

where

$$\mu'_* = \frac{\bar{\mu}_* - \beta}{1 - \beta \bar{\mu}_*} , \quad \bar{\phi}_* = \phi_* - \pi .$$

This can also be written in the form of the specific spectral photon density

$$n'_{bb}(\epsilon', \Omega') = \frac{u_*^0}{m_e c^2} \frac{\epsilon_*^2 \delta(\mu' - \mu'_*) \delta(\phi' - \bar{\phi}_*)}{[\exp(\epsilon_*/\Theta) - 1]} . \quad (\text{A2})$$

The nonthermal electrons Compton-scatter the target stellar photons that intercept the jet. The comoving-frame emissivity as a function of scattered photon energy ϵ'_s , scattered direction Ω'_s , and location x is given by

$$j'(\epsilon'_s, \Omega'_s; x) = m_e c^3 \epsilon'_s \int_0^\infty d\epsilon' \oint d\Omega' \int_1^\infty d\gamma \oint d\Omega'_e (1 - \beta_e \cos \psi') n'_{bb}(\epsilon', \Omega'; x) n'_e(\gamma, \Omega'_e) \left(\frac{d\sigma_C}{d\epsilon'_s d\Omega'_s} \right) \quad (\text{A3})$$

(Dermer et al. 1997). In this expression, $n'_e(\gamma, \Omega'_e) d\gamma d\Omega'_e$ is the differential number of electrons per unit proper volume in the comoving frame with Lorentz factors between γ and $\gamma + d\gamma$ that are directed into the solid angle element $d\Omega'_e$ in the direction Ω'_e , and ψ' is the angle between the incident photon and electron in the comoving frame. From Fig. 1b,

$$\cos \psi' = \mu' \mu'_e + \sqrt{1 - \mu'^2} \sqrt{1 - \mu_e'^2} \cos(\phi' - \phi'_e) ,$$

and $d\sigma_C/d\epsilon'_s d\Omega'_s$ is the differential Compton-scattering cross section. The speed of the electron is $\beta_e c$, and $\beta_e = \sqrt{1 - \gamma^{-2}} \approx 1$ for the relativistic electrons of interest in this problem.

Photons are scattered within a cone of half-opening angle $\approx 1/\gamma$ by electrons with $\gamma \gg 1$. For highly relativistic electrons, we employ the Compton-scattering cross section in the head-on approximation, where the scattered photons travel in the same direction as the scattering electrons. Thus

$$\frac{d\sigma_C}{d\epsilon'_s d\Omega'_s} = \frac{d\sigma_C}{d\epsilon'_s} \delta(\Omega'_s - \Omega'_e) ,$$

⁶ No primes are attached to the electron Lorentz factor γ , however, as this quantity is always referred to the comoving frame here.

and

$$\frac{d\sigma_C}{d\epsilon'_s} = \frac{3\sigma_T}{8\gamma\epsilon_i} \left[y + y^{-1} - \frac{2\epsilon'_s}{\gamma\epsilon_i y} + \left(\frac{\epsilon'_s}{\gamma\epsilon_i y} \right)^2 \right] H\left(\epsilon'_s; \frac{\epsilon_i}{2\gamma}, \frac{2\gamma\epsilon_i}{1+2\epsilon_i}\right) \quad (\text{A4})$$

(Jones 1968; Blumenthal & Gould 1970; Dermer & Schlickeiser 1993), where σ_T is the Thomson cross section, $H(x; a, b)$ is the Heaviside function such that $H(x; a, b) = 1$ if $a \leq x \leq b$ and $H(x; a, b) = 0$ otherwise, and

$$y \equiv 1 - \frac{\epsilon'_s}{\gamma} \quad \text{and} \quad \epsilon_i \equiv \gamma\epsilon'(1 - \beta_e \cos \psi') \cong \gamma\epsilon'(1 - \cos \psi'),$$

where ϵ'_s is the scattered photon energy in the comoving frame. The term ϵ_i gives the photon energy in the proper frame of the electron, and defines the regime of interaction (Thomson regime for $\epsilon_i \ll 1$, and KN regime for $\epsilon_i \gg 1$).

Substituting eqs. (A2) and (A4) into eq. (A3) gives, after solving the δ -functions, the result

$$j'(\epsilon'_s, \Omega'_s; x) = u_*^0 c \pi r_e^2 \epsilon'_s \int_1^\infty d\gamma \frac{n'_e(\gamma, \Omega'_s)}{\gamma^2} \int_{\epsilon'_l}^{\epsilon'_u} \frac{d\epsilon'}{\epsilon'} \frac{\epsilon_*^2}{\exp(\epsilon_*/\Theta) - 1} \left[y + y^{-1} - \frac{2\epsilon'_s}{\gamma\bar{\epsilon}_i y} + \left(\frac{\epsilon'_s}{\gamma\bar{\epsilon}_i y} \right)^2 \right], \quad (\text{A5})$$

where $\bar{\epsilon}_i = \gamma\epsilon'(1 - \cos \bar{\psi}')$,

$$\cos \bar{\psi}' = \mu'_* \mu'_s - \sqrt{1 - \mu'^2_*} \sqrt{1 - \mu'^2_s} \cos \bar{\phi}_*.$$

The equations relating the comoving and observer quantities are⁷

$$\epsilon'_s = \frac{(1+z)\epsilon}{\delta_D} \cong \frac{\epsilon}{\delta_D}, \quad \mu'_s = \frac{\mu - \beta}{1 - \beta\mu}, \quad \text{and} \quad \phi' = \phi.$$

The limits on the ϵ' -integral implied by the Heaviside function are

$$\epsilon'_l = \frac{\epsilon'_s}{2\gamma(\gamma - \epsilon'_s)(1 - \cos \bar{\psi}')} \quad \text{and} \quad \epsilon'_u = \frac{2\epsilon'_s}{1 - \cos \bar{\psi}'}.$$

The νF_ν spectrum resulting from Compton-scattered stellar radiation (CSSR) is given by

$$f_\epsilon^{C*} = \frac{\delta_D^4}{d_L^2} \epsilon'_s J'(\epsilon'_s, \Omega'_s) = \frac{\delta_D^4}{d_L^2} \epsilon'_s V'_b j'(\epsilon'_s, \Omega'_s), \quad (\text{A6})$$

where δ_D is the Doppler factor, eq. (4), V'_b is the comoving volume of the radiating region, and d_L is the luminosity distance to the source.

For a uniform emitting region filled with an isotropic comoving distribution of electrons,

$$V'_b n'_e(\gamma, \Omega'_s) = V'_b \frac{n'_e(\gamma)}{4\pi} = \frac{N'_e(\gamma)}{4\pi},$$

and we obtain eq. (3) for the CSSR spectrum. In this expression, we define

$$a = \Gamma(1 + \beta\mu'_*) , \quad b = \gamma(1 - \cos \bar{\psi}') \quad \text{and} \quad g = a/\Theta.$$

The integrals are defined as

$$I_i \equiv I_i(u_1) - I_i(u_2), \quad i = 1, 3,$$

where

$$I_1(u) = \int_u^\infty dx \frac{x}{\exp(x) - 1} \cong \begin{cases} \zeta(2) - u, & u \leq 1, \\ (1+u)\exp(-u), & u \geq 1, \end{cases} \quad (\text{A7})$$

$\zeta(n)$ is the Riemann zeta function ($\zeta(2) = \pi^2/6 = 1.6449\dots$), and

$$u_1 = a\epsilon'_l/\Theta \quad \text{and} \quad u_2 = a\epsilon'_u/\Theta.$$

The function I_2 is analytic and is given by

$$I_2 = \ln \left(\frac{1 - e^{-u_2}}{1 - e^{-u_1}} \right). \quad (\text{A8})$$

The function

$$I_3(u) = \int_u^\infty dx \frac{1}{x(e^x - 1)} \cong \frac{e^{-u}}{u}. \quad (\text{A9})$$

Fig. A1 compares the approximations for $I_1(u)$ and $I_3(u)$ with numerical integrations. These approximations, which introduce at most $\approx 10 - 20\%$ errors over a narrow range, are used in subsequent calculations.

⁷ The following results can be applied to sources at cosmological distances by replacing ϵ with $(1+z)\epsilon$ in the right-hand-sides of the subsequent expressions.

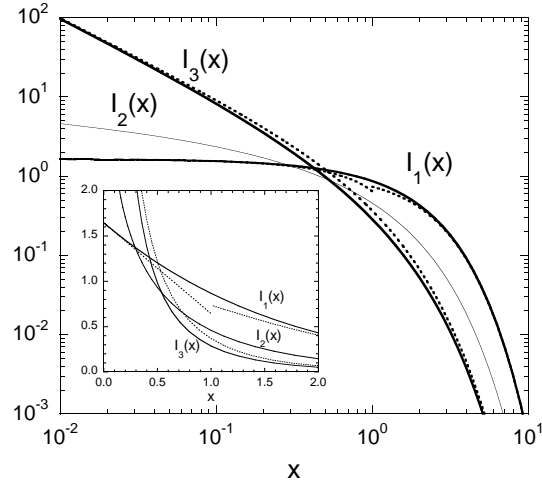


FIG. A7.— Solid curves are the integrals $I_1(u)$, $I_2(u)$, and $I_3(u)$ given by eqs. (A7) – (A9), and dotted curves are the approximations for $I_1(u)$ and $I_3(u)$ given by eqs. (A7) and (A9), respectively. Inset shows the comparison on a linear scale.

COMPARISON OF APPROXIMATIONS FOR RADIATION PROCESSES

Simpler expressions for the Compton-scattered photon spectrum from a point source can be derived using δ -function approximations for the Thomson and KN regimes in the head-on approximation (Dermer & Schlickeiser 1993). The accuracy of these expressions are indicated by comparing with accurate results obtained through numerical integrations of eqs. (3) and (6).

In the Thomson regime, we approximate the differential cross section by the expression

$$\frac{d\sigma_T}{d\epsilon'_s} = \sigma_T \delta(\epsilon'_s - \gamma\epsilon_i) H(1 - \epsilon_i), \quad (\text{B1})$$

where the Heaviside function with a single argument is defined by $H(x) = 1$ for $x \geq 0$, and $H(x) = 0$ otherwise. The Heaviside function in eq. (B1) obviously restricts scattering to the Thomson regime.

Following the approach leading to eq. (3), but now using cross section (B1) and approximating the star by a monochromatic point source with differential energy density

$$u_*(\epsilon_*, \Omega_*; r) = \hat{u}_* \delta(\epsilon_* - 2.70\Theta) \delta(\mu_* - \bar{\mu}_*) \delta(\phi_* - \bar{\phi}_*), \quad \hat{u}_* = \frac{L_*}{4\pi r^2 c},$$

we obtain the δ -function approximation to the CSSR νF_ν spectrum in the Thomson regime, given by

$$f_\epsilon^{T*} = \delta_D^4 \frac{c\sigma_T \hat{u}_* (1 - \beta\bar{\mu}_*)^2 (1 - \cos\bar{\psi}')^2 \Gamma^2}{8\pi d_L^2} \hat{\gamma}^3 N'_e(\hat{\gamma}) H\left[\frac{\delta_D}{2.70\Theta\Gamma(1 - \beta\bar{\mu}_*)(1 - \cos\bar{\psi}')} - \epsilon\right]. \quad (\text{B2})$$

Here

$$\hat{\gamma} = \sqrt{\frac{\epsilon}{2.70\Theta\Gamma\delta_D(1 - \beta\bar{\mu}_*)(1 - \cos\bar{\psi}')}},$$

$$\cos\bar{\psi}' = \mu'_* \mu'_s - \sqrt{1 - \mu_*'^2} \sqrt{1 - \mu_s'^2} \cos(\phi' - \bar{\phi}_*),$$

and, as before, $\mu'_* = (\bar{\mu}_* - \beta)/(1 - \beta\bar{\mu}_*)$ and $\mu'_s = (\mu - \beta)/(1 - \beta\mu)$. The factor 2.70 arises because the mean energy of a photon in a blackbody radiation field is $[3\zeta(4)/\zeta(3)]k_B T \cong 2.70k_B T$.

For a point source radiation field located behind the jet, $\bar{\mu}_* \rightarrow 1$ and $\cos\bar{\psi}' \rightarrow \mu'_s$. Replacing 2.70Θ with the dimensionless soft photon energy ϵ_0 , we obtain

$$f_\epsilon^{T,pt} = \delta_D^6 \frac{\sigma_T (1 - \mu)^2}{32\pi^2 x^2 d_L^2} \int_0^{1/\epsilon(1-\mu)} d\epsilon_0 L(\epsilon_0) \gamma_T^3 N'_e(\gamma_T) \quad (\text{B3})$$

(Dermer et al. 1992), where

$$\gamma_T = \frac{1}{\delta_D} \sqrt{\frac{\epsilon}{\epsilon_0(1 - \mu)}}.$$

This result is written in a form suitable for integration over the spectrum of an isotropic point source with spectral luminosity $L(\epsilon_0)$.

The beaming properties of the scattered spectrum are easily derived from eq. (B2). If $N'_e(\gamma) \propto \gamma^{-p}$, then

$$f_\epsilon^{T*} \propto \delta_D^{(5+p)/2} [\Gamma(1 - \beta\bar{\mu}_*)(1 - \cos\bar{\psi}')]^{(p+1)/2} (\epsilon/\epsilon_0)^{(3-p)/2}. \quad (B4)$$

For a point source behind the jet, $\bar{\mu}_* \rightarrow 1$, and $[\dots] \rightarrow \delta_D(1 - \mu)$ in eq. (B4), so that

$$f_\epsilon^{T,pt} \propto \delta_D^{3+p}(1 - \mu)^{(p+1)/2} (\epsilon/\epsilon_0)^{(3-p)/2}.$$

For a point source in front of the jet, $\bar{\mu}_* \rightarrow -1$, and $[\dots] \rightarrow \delta_D(1 + \mu)$ in eq. (B4), so that

$$f_\epsilon^{T,ptf} \propto \delta_D^{3+p}(1 + \mu)^{(p+1)/2} (\epsilon/\epsilon_0)^{(3-p)/2},$$

which has the same beaming dependence as an external isotropic photon field (Dermer 1995). Because these results span the possible locations of the stellar point source radiation field, we see that the principal dependence of the beaming factor in the Thomson regime is $f_\epsilon^{T*} \propto \delta_D^{3+p}(\epsilon/\epsilon_0)^{(3-p)/2}$ multiplied by an angle-dependent factor; the exact beaming factor for the CSSR process in the Thomson regime is given by eq. (B4).

In the KN regime, we use the δ -function approximation

$$\frac{d\sigma_{KN}}{d\epsilon'_s} = \frac{3\sigma_T}{8\epsilon_i} \ln(2e^{1/2}\epsilon_i)\delta(\epsilon'_s - \gamma)H(\epsilon_i - 1) \quad (B5)$$

(Dermer & Schlickeiser 1993; Li & Wang 2004) for the cross section. The CSSR νF_ν spectrum of point-source emission scattered by a jet in the KN regime is given for approximation (B5) by the expression

$$f_\epsilon^{KN*} = \delta_D^6 \frac{3c\sigma_T \hat{u}_* \gamma_{KN}^3 N'_e(\gamma_{KN})}{32\pi d_L^2 (2.70\Theta)^2 \epsilon^2} \ln[2e^{1/2}\gamma_{KN} \cdot 2.70\Theta\Gamma(1 - \beta\bar{\mu}_*)(1 - \cos\bar{\psi}')] \times \\ H\left[\epsilon - \frac{\delta_D}{2.70\Theta\Gamma(1 - \beta\bar{\mu}_*)(1 - \cos\bar{\psi}')}\right], \quad (B6)$$

where

$$\gamma_{KN} = \frac{\epsilon}{\delta_D}. \quad (B7)$$

The KN regime νF_ν spectrum of an isotropically emitting point-source of radiation located behind the jet is given by the expression

$$f_\epsilon^{KN} = \delta_D^6 \frac{3\sigma_T \gamma_{KN}^3 N'_e(\gamma_{KN})}{128\pi^2 x^2 d_L^2 \epsilon^2} \int_{1/\epsilon(1-\mu)}^\infty d\epsilon_o \frac{L(\epsilon_o)}{\epsilon_o^2} \ln[2e^{1/2}\epsilon\epsilon_o(1 - \mu)]. \quad (B8)$$

The principal dependence of the beaming factor in the KN regime for a point source behind (−) and in front of (+) of the jet, from eqs. (B6) and (B7) and the results following eq. (B4), goes as

$$f_\epsilon^{KN} \propto \delta_D^{3+p} \ln[\epsilon\epsilon_0(1 \pm \mu)]\epsilon^{1-p}. \quad (B9)$$

Because of the slowly varying logarithmic factor, the Doppler dependence of the beaming factor in the KN regime goes as $f_\epsilon^{KN} \propto \delta_D^{3+p}$, as in the case for a surrounding isotropic external radiation field (Georganopoulos et al. 2001).

Fig. B1 gives a comparison of the δ -function (dotted lines) approximations and the accurate (solid curves) calculations of the CSSR and CSAD processes, respectively. The lower and upper branches of the approximations for the CSSR and CSAD processes represent the Thomson and KN δ -function approximations, respectively. Here we treat a monochromatic point source of radiation that radiates isotropically from behind a one-sided jet with Lorentz factor $\Gamma = 2$. The parameters of the stellar radiation field and accretion disk point source are given by Table 1 parameter study values, though here we use only a single power-law electron distribution between electron Lorentz factors $\gamma = 10^2$ and 10^8 with $p = 2.5$. The accretion disk luminosity is 10^{36} ergs s $^{-1}$, and the accretion disk is assumed to emit monochromatically at 1 keV. The emission from this source is plotted as a thermal emitter with effective temperature $\Theta_{pt} = 1.0/(2.70 \times 511)$. Depending on the accuracy desired, the δ -function approximations may be adequate for calculating the spectrum of a point-source radiation field, and is simpler when integrating over non-monochromatic accretion-disk radiation spectra.

It is also useful to compare simple δ -function approximations for the synchrotron and SSC processes with more accurate calculations. A δ -function approximation for the synchrotron spectrum is

$$f_\epsilon^{\text{syn}} \cong \frac{\delta_D^4}{6\pi d_L^2} c\sigma_T u'_B \gamma_s^3 N'_e(\gamma_s), \quad \gamma_s = \sqrt{\frac{\epsilon'}{\delta_D \epsilon_B}}, \quad (B10)$$

where $\epsilon_B = B(G)/4.414 \times 10^{13}$ G, and $B(G)$ is the magnetic field in the comoving frame. A δ -function approximation for the SSC spectrum is

$$f_\epsilon^{\text{SSC}} \cong \delta_D^4 \frac{c\sigma_T^2 r_b u'_B}{12\pi d_L^2 V'_b} \left(\frac{\epsilon'}{\epsilon_B}\right)^{3/2} \int_0^{\min(\epsilon', 1/\epsilon')} d\epsilon'_i \epsilon'_i{}^{-1} N'_e(\sqrt{\frac{\epsilon'}{\epsilon'_i}}) N'_e(\sqrt{\frac{\epsilon'_i}{\epsilon_B}}) \quad (B11)$$

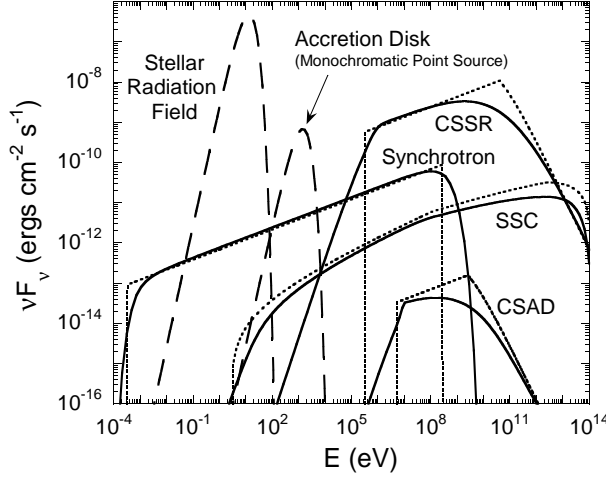


FIG. B8.— Spectra of stellar and accretion-disk radiation fields (long-dashed curves), and accurate and approximate calculations of the spectral components emitted by a one-sided microquasar jet. The jet spectral components include the synchrotron spectrum, the synchrotron self-Compton (SSC) spectrum, the Compton-scattered stellar radiation (CSSR) spectrum, and the Compton-scattered accretion disk (CSAD) spectrum. Accurate calculations for the synchrotron spectrum, the SSC spectrum, and the CSSR and CSAD spectra in the head-on approximation are shown by the solid curves, whereas δ -function approximations are shown by the dotted lines and curves. The parameters of the calculation are given by the parameter study values in Table 1, except that here the electron spectrum is a single power law with spectral index $p = 2.5$ for $10^2 \leq \gamma \leq 10^8$, and $\phi = 0$.

(Dermer & Schlickeiser 2002), where $u'_B = B^2/8\pi$ and $V'_b = 4\pi r_b^3/3$. The only provision made in this approximation to account for scattering in the KN regime is to terminate the scattering when $\gamma\epsilon'_i \geq 1$.

For the broken power-law electron distribution, eq. (7), eq. (B11) gives

$$f_\epsilon^{\text{SSC}} \cong \delta_D^4 \frac{c\sigma_T^2 u'_B}{16\pi^2 d_L^2 r_b^2} K^2 \left(\frac{\epsilon'}{\epsilon_B} \right)^{3/2} [\gamma_1^{2(q-p)} \mathcal{I}_1 + \gamma_1^{q-p} (\mathcal{I}_2 + \mathcal{I}_3) + \mathcal{I}_4], \quad (\text{B12})$$

where

$$\begin{aligned} \mathcal{I}_1 &= \left(\frac{\epsilon'}{\epsilon_B} \right)^{-q/2} \ln \left[\frac{\min(\epsilon'^{-1}, \epsilon'/\gamma_0^2, \epsilon_B \gamma_1^2)}{\max(\epsilon'/\gamma_1^2, \epsilon_B \gamma_0^2)} \right], \\ \mathcal{I}_2 &= \frac{2\epsilon_B^{q/2} \epsilon'^{-p/2}}{p-q} \left\{ [\min(\epsilon'^{-1}, \epsilon'/\gamma_1^2, \epsilon_B \gamma_1^2)]^{(p-q)/2} - [\max(\epsilon'/\gamma_2^2, \epsilon_B \gamma_0^2)]^{(p-q)/2} \right\}, \\ \mathcal{I}_3 &= \frac{2\epsilon_B^{p/2} \epsilon'^{-q/2}}{q-p} \left\{ [\min(\epsilon'^{-1}, \epsilon'/\gamma_0^2, \epsilon_B \gamma_2^2)]^{(q-p)/2} - [\max(\epsilon'/\gamma_1^2, \epsilon_B \gamma_1^2)]^{(q-p)/2} \right\}, \text{ and} \\ \mathcal{I}_4 &= \left(\frac{\epsilon'}{\epsilon_B} \right)^{-p/2} \ln \left[\frac{\min(\epsilon'^{-1}, \epsilon'/\gamma_1^2, \epsilon_B \gamma_2^2)}{\max(\epsilon'/\gamma_2^2, \epsilon_B \gamma_1^2)} \right] \end{aligned}$$

(see also Tavecchio et al. 1998). In deriving this expression, we assume that the mean escape time of a synchrotron photon from the uniform spherical emitting region is $3r_b/4c$.

The quality of the δ -function approximations for the synchrotron and SSC processes is shown in Fig. B1. Note that synchrotron self-absorption plays a role at the lowest synchrotron photon energies, and is not considered in the approximate curve.

ALLOWED PARAMETERS FOR LEPTONIC JET MODEL FROM RADIATION REACTION LIMIT

We first generalize the well-known expression for the maximum electron Lorentz factor obtained by comparing the optimal Fermi acceleration rate with the synchrotron energy-loss rate (Guilbert et al. 1983; Rachen & Mészáros 1998) to include Compton losses on the CSSR field. Besides treating KN effects on the energy-loss rates (Aharonian et al. 2005a), our results also correct for relativistic jet motions on the Doppler-boosted stellar radiation field.

The electron gyration frequency $\omega_g = eB/m_e c \gamma$ in a magnetic field with mean intensity B . Note a number of underlying assumptions in this treatment: that the mean magnetic field is uniform throughout the emitting volume, and that it is randomly oriented. The acceleration rate ω_{acc} in Fermi processes cannot exceed the gyration frequency because an electron gains at most a fraction of its energy when executing a single gyration in first-order shock or

second-order stochastic Fermi processes. Thus $\omega_{acc} = \eta\omega_g$, with $\eta \lesssim 1$. The fractional synchrotron energy-loss rate $\omega_{syn} = |-\dot{\gamma}_{syn}/\gamma| = \sigma_T B^2 \gamma / 6\pi m_e c$ which, when equated with the acceleration rate, gives

$$\gamma_{max} = \eta^{1/2} \sqrt{\frac{6\pi e}{\sigma_T B}} \cong \frac{1.2 \times 10^8 \eta^{1/2}}{\sqrt{B(\text{G})}}, \quad (\text{C1})$$

and a maximum synchrotron frequency of $h\nu_{max} \cong \delta_D (\hbar e B / m_e c) \gamma^2 / (1+z) \cong 160 \eta \delta_D / (1+z)$ MeV.

Scattering in the Klein-Nishina regime is important when $4\gamma\epsilon' = 4\gamma[2.70\Theta\Gamma(1-\beta\bar{\mu}_*)] \gtrsim 1$ (compare eq. [10]), that is, when $\gamma \gtrsim 5 \times 10^4 / [k_B T_*(\text{eV})\Gamma(1-\beta\bar{\mu}_*)]$. The fractional energy-loss rate in the extreme KN regime for a blackbody radiation field with dimensionless temperature Θ is

$$\omega_{KN} = \left| \frac{-\dot{\gamma}_{KN}}{\gamma} \right| \cong \frac{c\sigma_T}{16\lambda_C^3} \frac{\Theta^2}{\gamma} \ln(0.552\gamma\Theta) \quad (\text{C2})$$

(Blumenthal & Gould 1970), where $\lambda_C = \lambda_C / 2\pi = \hbar / m_e c = 3.86 \times 10^{-11}$ cm is (also called) the electron Compton wavelength.

The energy density u'_* of a stellar blackbody radiation field in the comoving jet frame has to be corrected by a graybody factor that accounts for (1) the dilution of the radiation field due to the distance of the jet from the star, and (2) the reduction in energy density due to the bulk relativistic motion of the jet. Recalling that the energy density at the surface of a blackbody is 1/4 times the energy density in the interior of a blackbody cavity, the relation between the energy densities is therefore given by

$$u'_* = \frac{1}{4} \left(\frac{R_*}{r} \right)^2 \Gamma^2 (1 - \beta\bar{\mu}_*)^2 u_{bb}(\Theta) \quad (\text{C3})$$

(e.g., Dermer & Schlickeiser 2002), where $u_{bb}(\Theta) = \pi^2 m_e c^2 \Theta^4 / 15 \lambda_C^3$ is the energy density of a blackbody stellar radiation field with dimensionless temperature Θ .

The graybody factor from eq. (C3) therefore gives the maximum electron Lorentz factor γ_{max} by solving the equation

$$\eta \frac{eB}{m_e c} = \frac{\sigma_T B^2 \gamma_{max}^2}{6\pi m_e c} + \left(\frac{R_*}{r} \right)^2 \Gamma^2 (1 - \beta\bar{\mu}_*)^2 \frac{c\sigma_T}{64\lambda_C^3} \Theta^2 \ln[0.552\gamma_{max}\Gamma\Theta(1 - \beta\bar{\mu}_*)]. \quad (\text{C4})$$

which holds when $\gamma_{max} \gg [\Gamma\Theta(1 - \beta\bar{\mu}_*)]^{-1}$. The maximum synchrotron energy in the comoving frame is $h\nu'_{max,syn} \cong (\hbar e B / m_e c) \gamma_{max}^2$. Eq. (C4) can be rewritten as

$$\gamma_{max}^2 = \eta \frac{9B_{cr}}{4\alpha_f B} - \frac{3\pi\alpha_f}{32} \left(\frac{B_{cr}}{B} \right)^2 \left[\frac{R_* \Gamma(1 - \beta\bar{\mu}_*) \Theta}{r} \right]^2 \ln[0.552\gamma_{max}\Gamma\Theta(1 - \beta\bar{\mu}_*)], \quad (\text{C5})$$

where $\alpha_f = 1/137$ is the fine structure constant and $B_{cr} = m_e^2 c^3 / e \hbar = 4.41 \times 10^{13}$ G is the critical magnetic field. Again, this expression holds as long as the argument of the logarithm is much greater than unity.

Because of the similar dependence of the acceleration rate and the fractional KN energy-loss rate found in eq. (C4), Compton-scattering in the KN regime will be unimportant to limit electron acceleration when

$$\frac{r}{R_*} \gtrsim \alpha_f \Theta \sqrt{\frac{\pi B_{cr}}{24\eta B}} \cong 0.07 \frac{T_*(\text{eV}) \Gamma(1 - \beta\bar{\mu}_*)}{\sqrt{\eta B(\text{G})}}; \quad (\text{C6})$$

here we have taken the square root of the logarithmic term ≈ 2 .

A limit on the range of values of B can be obtained by noting that the emission of photons with energy E_γ requires electrons with Lorentz factors

$$\gamma \gtrsim \frac{E_\gamma}{\delta_D m_e c^2} \cong \frac{2 \times 10^7 E_{10}}{\delta_D},$$

where $E_{10} \equiv E_\gamma / 10$ TeV. From Eq. (C1),

$$B(\text{G}) \lesssim 38\eta \delta_D^2 / E_{10}^2. \quad (\text{C7})$$

With eq. (C6), this implies an allowed range of magnetic fields, given by

$$\frac{5 \times 10^{-3}}{\eta} T_*^2(\text{eV}) \left[\frac{R_* \Gamma(1 - \beta\bar{\mu}_*)}{r} \right]^2 \lesssim B(\text{G}) \lesssim \frac{38\eta \delta_D^2}{E_{10}^2}, \quad (\text{C8})$$

for a leptonic jet model to apply to the observed VHE emission from a microquasar.

For the parameters of LS 5039 given in Table 1,

$$\frac{0.024}{\eta} \frac{[\Gamma(1 - \beta\bar{\mu}_*)]^2}{r_{12}^2} \lesssim B(\text{G}) \lesssim \frac{38\eta \delta_D^2}{E_{10}^2}, \quad (\text{C9})$$

where $r_{12} = r / 10^{12}$ cm and $\bar{\mu}_* = \sqrt{1 - d^2/r^2}$. For a nonrelativistic outflow, as treated by Aharonian et al. (2005a), $\eta \rightarrow \eta_0 \beta^2 = (0.2)^2 \eta_0 (\beta/0.2)^2$, with $\eta_0 \lesssim 1$. The allowed range becomes

$$\frac{0.6}{\eta_0 r_{12}^2 (\beta/0.2)^2} \lesssim B(\text{G}) \lesssim \frac{1.4\eta_0 (\beta/0.2)^2}{E_{10}^2}. \quad (\text{C10})$$

If the jet is nonrelativistic, eq. (C10) circumscribes the mean comoving magnetic field of a leptonic jet model for LS 5039 to a narrow range of values unless $r_{12} \gg 1$ even for the optimistic case of $\eta_0 \cong 1$, in which case the orbital modulation of the γ -ray emission due to $\gamma\gamma$ attenuation and, to a lesser extent, the CSSR process will be small. Even a mildly relativistic jet ($\Gamma \gtrsim 1.5$) opens up a much larger allowable parameter space to permit the source of emission to originate from the inner jet. Note that the inferred jet speed from radio observations (Paredes et al. 2002) of LS 5039 may not be representative of the jet speed near the source due to bulk deceleration caused, for example, by radiative drag.

ALLOWED PARAMETERS FOR LEPTONIC JET MODEL FROM RATIO OF COMPTON TO SYNCHROTRON FLUXES

A further restriction on parameters for a leptonic microquasar jet model can be obtained by noting that the ratio of the peak νF_ν fluxes for the Compton and synchrotron components, denoted by ρ , is related to the ratio of the comoving photon u'_* and magnetic field u'_B energy densities by the relation

$$\rho \equiv \frac{f_{\epsilon_{pk,C}}^C}{f_{\epsilon_{pk,s}}^S} \approx \frac{u'_*}{u'_B} \quad (D1)$$

(compare Sikora 1997, for blazars). This expression, which neglects angular scattering effects, holds for scattering in the Thomson regime and so would best be applied to emission observed in the GLAST band. Taking

$$u'_* = \frac{L_*}{4\pi r^2 c} \Gamma^2 (1 - \beta \bar{\mu}_*)^2,$$

(compare eq. [C3]; $\sigma_{SB} = \pi^2 m_e c^3 k_B^4 / [60 \lambda_C^3 (m_e c^2)^4]$), we find

$$r \gtrsim \frac{E_{10}^2}{38 \eta \delta_D^2} \left(\frac{2L_*}{c\rho} \right)^{1/2} \Gamma (1 - \beta \bar{\mu}_*). \quad (D2)$$

using eq. (C7). For the parameters of LS 5039,

$$r_{12} \gtrsim \frac{0.6 E_{10}^2}{\eta \sqrt{\rho/100}} \frac{\Gamma (1 - \beta \bar{\mu}_*)}{\delta_D^2} \rightarrow \frac{15 E_{10}^2}{\eta_0 (\beta/0.2)^2 \sqrt{\rho/100}}, \quad (D3)$$

where the last expression holds for a nonrelativistic outflow. Application of this constraint implies that we properly identify the peak nonthermal jet synchrotron flux, which is not necessarily obvious from the broadband data (see Fig. 5). Choosing a value $\rho \approx 10^2$ suggested by Fig. 6 data, we conclude that emission from the inner jet is possible for a mildly relativistic leptonic jet model, but not for a nonrelativistic jet at the base of the microquasar.

REFERENCES

- Aharonian, F., et al., 2005, *Science*, 309, 746
 Aharonian, F., Anchordoqui, L. A., Khangulyan, D., & Montaruli, T., 2005a, *astro-ph/0508658*
 Atoyan, A. M., & Aharonian, F. A. 1999, *MNRAS*, 302, 253
 Bednarek, W. 1997, *A&A*, 322, 523
 Begelman, M. C., & Sikora, M. 1987, *ApJ*, 322, 650
 Blumenthal, G. R., & Gould, R. J. 1970, *Reviews of Modern Physics*, 42, 237
 Böttcher, M., & Dermer, C. D. 2005, *ApJ Letters*, 634, L81
 Bosch-Ramon, V., Paredes, J. M., Ribó, M., Miller, J. M., Reig, P., & Martí, J. 2005, *ApJ*, 628, 388
 Bosch-Ramon, V., Romero, G. E., & Paredes, J. M. 2005a, *A&A*, 429, 267
 Bosch-Ramon V., Romero, G. E., & Paredes, J. M. 2005b, *A&A*, in press (*astro-ph/0509086*)
 Bosch-Ramon, V., Aharonian, F. A., & Paredes, J. M. 2005c, *A&A*, 432, 609
 Bosch-Ramon, V., & Paredes, J. M., 2004a, *A&A*, 417, 1075
 Bosch-Ramon, V., & Paredes, J. M. 2004b, *A&A*, 425, 1069
 Butt, Y. M., Maccarone, T. J., & Prantzos, N. 2003, *ApJ*, 587, 748
 Casares, J., Ribó, M., Ribas, I., Paredes, J. M., Martí, J., & Herrero, A., 2005, *MNRAS*, 364, 899
 Dermer, C. D. 1995, *ApJ*, 446, L63
 Dermer, C. D., Schlickeiser, R., & Mastichiadis, A. 1992, *A&A*, 256, L27
 Dermer, C. D. & Schlickeiser, R. 1993, *ApJ*, 416, 458
 Dermer, C. D., Sturmer, S. J., & Schlickeiser, R. 1997, *ApJS*, 109, 103
 Dermer, C. D., & Schlickeiser, R. 2002, *ApJ*, 575, 667
 Dermer, C. D., & Atoyan, A. M. 2002, *ApJ*, 568, L81
 Dubus, G., 2005, *A&A*, submitted (*astro-ph/0509633*)
 Fender, R., & Maccarone, T. 2004, *ASSL Vol. 304: Cosmic Gamma-Ray Sources*, K.S. Cheng and G.E. Romero (eds.), (Kluwer: Dordrecht), p. 205 (*astro-ph/0310538*)
 Georganopoulos, M., Aharonian, F. A., & Kirk, J. G. 2002, *A&A*, 388, L25
 Georganopoulos, M., Kirk, J. G., & Mastichiadis, A. 2001, *ApJ*, 561, 111; (e) 2004, *ApJ*, 604, 479
 Gregory, P. C., & Taylor, A. R., 1978, *Nature*, 272, 704
 Grenier, I. A., Casandjian, J.-M., & Terrier, R. 2005a, *Science*, 307, 1292
 Grenier, I. A., Bernadó, M. M. K., & Romero, G. E. 2005a, *Ap&SS*, 297, 109
 Guilbert, P. W., Fabian, A. C., & Rees, M. J. 1983, *MNRAS*, 205, 593
 Gupta, S., Böttcher, M., & Dermer, C. D. 2005, *ApJ*, submitted
 Hermesen, W., et al. 1977, *Nature*, 269, 494
 Jones, F. C. 1968, *Physical Review*, 167, 1159
 Kaufman Bernadó, M. M., Romero, G. E., & Mirabel, I. F. 2002, *A&A*, 385, L10
 Kniffen, D. A., et al. 1997, *ApJ*, 486, 126
 Levinson, A. & Blandford, R. 1996, *ApJ*, 456, L29
 Li, H., & Wang, J. 2004, *ApJ*, 617, 162
 Markoff, S., Falcke, H., & Fender, R. P. 2001, *A&A*, 372, L25
 Markoff, S., Nowak, M., Corbel, S., Fender, R., & Falcke, H. 2003, *A&A*, 397, 645
 Massi, M. 2004, *A&A*, 422, 267
 McSwain, M. V., Gies, D. R., Riddle, R. L., Wang, Z., & Wingert, D. W. 2001, *ApJ*, 558, L43
 Melia, F., & Königl, A. 1989, *ApJ*, 340, 162
 Paredes, J. M. 2005, *Chinese Journal of Astronomy and Astrophysics*, 5, 121 (*astro-ph/0409226*)

TABLE D1
STANDARD VALUES USED IN PARAMETER STUDY AND MODEL FITS TO LS 5039

Quantity	Parameter	Model A	Model B
	Study		
d_L (kpc)	3.0		
T_* (K)	39000		
L_* (ergs s $^{-1}$)	7×10^{38}		
R_* (cm)	6.5×10^{11}		
d (cm)	2.5×10^{12}		
θ (incl.)	25°		
Γ	2.0		
δ_D	2.32		
B (G)	1.0	0.8	0.8
r_b (cm)	10^{11}	2×10^{11}	10^{11}
W'_e (ergs)	10^{38}	2×10^{37}	2×10^{38}
p	3.0	2.25	3.0
q	2.0	1.25	2.0
γ_0	100	10	300
γ_1	10^3	100	10^3
x (cm)	2.5×10^{12}	2×10^{13}	$10^{13}, 10^{14}$
L_{pt} (ergs s $^{-1}$)	10^{36}	–	10^{34}
T_{pt} (keV)	1/2.70	–	0.3/2.70

Paredes, J. M., Martí, J., Ribó, M., & Massi, M. 2000, *Science*, 288, 2340
Paredes, J. M., Ribó, M., Ros, E., Martí, J., & Massi, M. 2002, *A&A*, 393, L99
Paredes, J. M., Bosch-Ramon, V., & Romero, G. E., 2005, *A&A*, in press (astro-ph/0509095)
Protheroe, R. J., Mastichiadis, A., & Dermer, C. D. 1992, *Astroparticle Physics*, 1, 113
Rachen, J. P., and Mészáros, P. 1998, *Phys. Rev. D*, 58, 123005.
Ribó, M., Reig, P., Martí, J., & Paredes, J. M. 1999, *A&A*, 347, 518
Rieger, F. M. 2004, *ApJ*, 615, L5
Romero, G. E., Torres, D. F., Kaufman Bernadó, M. M., & Mirabel, I. F., 2003, *A&A*, 410, L1
Romero, G. E., Christiansen, H. R., & Orellana, M. 2005, *ApJ*, 632, 1093

Romero, G. E. 2005, *Chinese Journal of Astronomy and Astrophysics*, 5, 110 (astro-ph/0407461)
Sikora, M., Begelman, M. C., & Rees, M. J. 1994, *ApJ*, 421, 153
Sikora, M. 1997, *AIP Conf. Proc.* 410: Proceedings of the Fourth Compton Symposium, 410, 494
Tavani, M., Kniffen, D., Mattox, J. R., Paredes, J. M., & Foster, R. 1998, *ApJ*, 497, L89
Tavecchio, F., Maraschi, L., & Ghisellini, G. 1998, *ApJ*, 509, 608
Torres, D. F., Romero, G. E., Dame, T. M., Combi, J. A., and Butt, Y. M. 2003, *Phys. Reports*, 382, 303
Torres, D. F., Romero, G. E., Barcons, X., & Lu, Y., 2005, *ApJ*, 626, 1015